山形大学紀要（工学）第 37 巻　平成 30 年 8 月
Bull. Yamagata Univ. (Eng.) Vol. 37 Aug. 2018

Agent-based simulation of the collective behavior of actin filaments depending on driving and packing forces

Kuniyuki HATORI, Takahiro IWASE

Department of Bio-Systems Engineering, Graduate School of Science and Engineering, Yamagata University, Yonezawa 992-8510, Japan

（平成 30 年 1 月 9 日受付，平成 30 年 5 月 18 日受理）

Abstract

The sliding movement of actin filaments driven by myosin motors, which underlies muscle contractions, can be observed by microscopy when purified actin and myosin are combined in vitro. At a low actin filament density, individual filaments move in random directions, whereas in condensed conditions, actin filaments gather together and are oriented in parallel. We have revealed that crowded conditions due to the presence of methylcellulose induce the alignment of bands so that actin filaments converge with collective movement (Iwase, T. et al., Biochim. Biophys. Acta 1861, pp. 2717–2725, 2017). The bands aligned at regular intervals, which seem to be determined by sliding velocity, driving force, and packing force. To understand the formation mechanism, we here present an agent-based simulation for these factors. The simulation suggests that obvious alignment of actin filaments occurs under the same magnitude of driving and packing forces, as expected in physiological conditions.

Keywords: Actomyosin; Collective motion; Soft matter; Self-organization; Biophysics

1. Introduction

Organization of cytoskeleton components such as the bundle formations of actin filaments occurs in cells during their migration and cytokinesis[1,2]. Skeletal muscle cells contain highly aligned actin and myosin filaments, and their synergy is required for contractions. Although collectivity is a widely recognized organization pattern for a swarm of microorganisms, it remains unclear how collectivity arises from the stochastic behavior of protein interactions. The motility of actin filaments driven by myosin motor proteins during the hydrolysis of adenosine triphosphate (ATP), which underlies muscle contractions, can be evaluated in an in vitro motility assay[3]. This assay has been developed for the visualization of single actin

filaments under a fluorescence microscope, in which fluorescently labeled actin filaments and ATP are applied on a myosin-coated glass slide for observing sliding movement. In this reconstitution system, the collective movement of actin filaments, in which numerous filaments proceed in the same direction, has been disclosed when the surface density of the filaments reaches up to 20 filaments per square micrometer[4,5]. Similar behavior was also observed in the case of a condensed kinesin-microtubule system, another type of motor protein[6,7]. Therefore, collective movement might be universal for all types of autonomously propelling matter[8]. We recently identified another type of collective phenomenon by which myosin-driven actin filaments gather into stream bands that tend to align at regular intervals in the presence of methylcellulose (MC), which serves as a crowder at near physiological ionic strength[9], as depicted in Fig. 1. Such crowded conditions can induce an attraction force between actin filaments via an entropic effect, namely an excluded volume effect[10], whereas high ionic conditions decrease the magnitude of the driving force between the actin filaments and myosin motor domains due to weakening of their electrostatic interactions[11]. Therefore, it is possible that the alignment pattern forms in response to a balance between the driving force and attraction force that can pack the

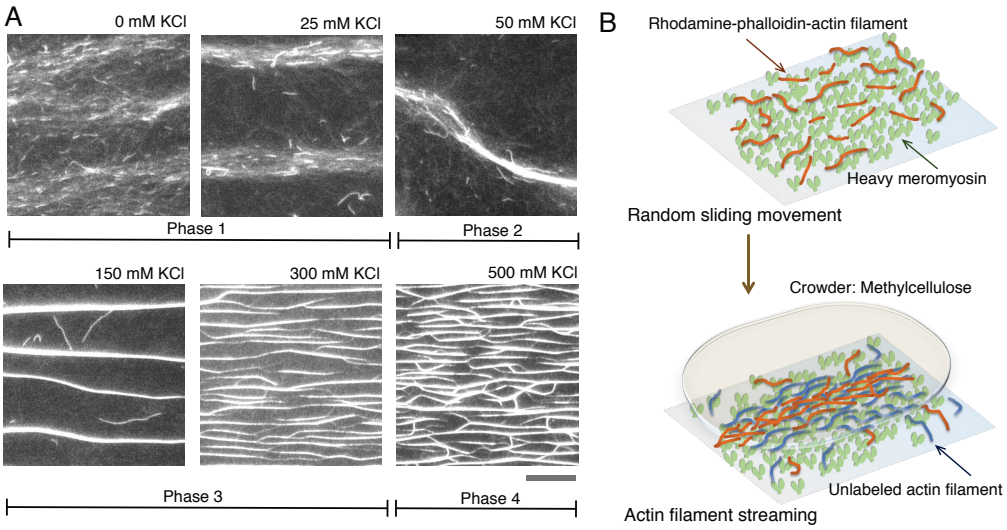

Figure 1: Alignment of actin filament streams driven by myosin motors in the presence of MC using an in vitro motility system. (A) The feature of actin filament streams alters in response to changes in KCl concentrations. The patterns were classified into four phases. Scale bar at the bottom right of the image, 10 μm. (B) Schematic diagram of the movement of actin filaments from a random to collective pattern. Individual actin filaments were driven by ATP-activated myosin motors coated on a glass slide. Conditions: 0.2 mg/mL actin filaments, 1 μg/mL tetramethyl rhodamine phalloidin-bound actin filaments, 25 mM imidazole-HCl (pH 7.4), 4 mM $MgCl_2$, 0.5% 2-mercaptoethanol, 1 mM ATP, 1% MC, and variable concentrations of KCl. Reprinted from Fig. 2 and Fig. 3A of Iwase et al.[9], Copyright 2017, with permission from Elsevier.

filaments. In addition, the space intervals between stream bands seem to be correlated with the sliding velocity. To verify this hypothesis, we carried out an agent-based simulation for the formation of stream bands composed of myosin-driven filaments by varying the settings of the driving and packing forces as well as velocity.

2. Methods

2.1 Agent-based simulation of the movement of actin filaments

In a standard motility assay, individual actin filaments are non-directionally translocated by myosin motors because the myosin molecules are randomly fixed on a glass surface. Filament velocity depends on myosin activity, ionic strength, and other factors. However, the velocity is independent of filament length. On the basis of these properties, we simulated the motility of actin filaments on a computer (Fig. 2). Figure 3A displays the overall design of our agent-based model. Actin filaments were moved at intervals of 0.1 s with both velocity and angle fluctuations (Gaussian distribution) based on experimental data[12]. The standard deviations (SDs) for velocity and angle were set at ±15% of average velocity and ±14°, respectively. The direction angle was restricted within ±14° while moving the left path persistence length (8 μm) unless a packing effect was applied. Average velocity was varied in the range of 2–8 μm/s in response to KCl concentrations (see Sec. 2.3). The length of all filaments was fixed at 1 μm, and the whole area was set to 60 μm × 60 μm. We designed the model so that when filaments exit on one edge they re-enter through the opposite edge. The total filament number was set to 15,000, and 15% of them were visualized as a standard.

2.2 Constraint on movement by the packing effect

The presence of crowders leads to associations between proteins. Our previous study demonstrated that moving actin filaments driven by myosin motors tend to assemble into bundles or stream bands in the presence of 1% (w/v) MC. Therefore, in the present simulation, an attraction force between filaments (packing force) was assumed in addition to a driving force. To apply constraints in terms of the packing force, the entire local area was established as a divided search area (2 μm × 2 μm), and four main constraints were applied: density constraint, direction change constraint, translation constraint, and initial constraint. For the density constraint, the direction of filaments was changed when the ratio of the filament density in the search area to the average density exceeded a threshold value (defined parameter, E), which was usually

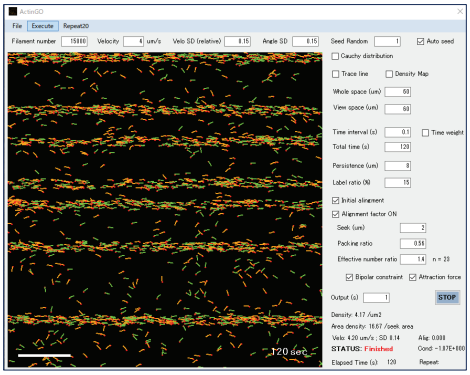

Figure 2: Interface of the simulator programed in Microsoft Visual C#.

assigned to be 1.4. For the direction change constraint, the direction was categorized into 8 sub-divisions at intervals of 45° in the search area. The division of the largest population of filaments was selected, and the reference direction was determined from the average directions of individual filaments in the selected division (Fig. 3B). The direction of all filaments in the search area was shifted toward the reference axis by the packing ratio (parameter, P), which was defined as the degree of changing direction ($P = \Delta\theta/\theta$, where theta is the angle between the filament direction and reference axis), as depicted in Fig. 3C. We assumed that P is determined by a balance between driving and packing forces (see Sec. 2.3). In this condition, a further assumption of bidirectional permission was applied with respect to the rotation direction. If the filament direction was within the range of –90° to 90° on the basis of the reference direction (0°), the filament direction shifted toward the reference, whereas in the range of 90° to 270°, the direction shifted toward the opposite direction of the reference (180°). For the translation constraint, a filament was translated into the nearest filament by a bias distance ($\Delta d = d \times P \times \cos\phi$, where d and ϕ denote the distance and the angle between two filaments, respectively), as depicted in Fig. 3D.

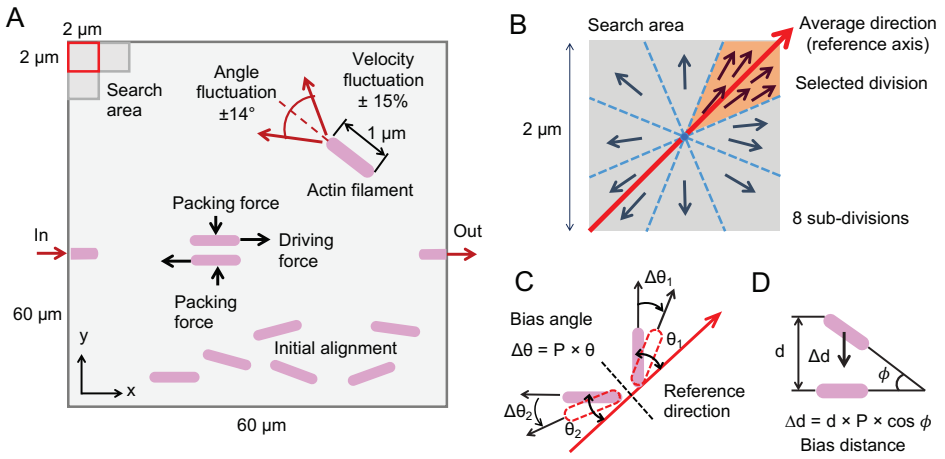

Figure 3: Design for the simulation of the movement of actin filaments with driving and packing forces. (A) Working area and movement of individual filaments. Constant parameters: velocity and angle fluctuations, 15% and 14° as SDs in Gaussian distribution, respectively; whole area, 60 μm × 60 μm; search area, 2 μm × 2 μm; filament number, 15,000 (density 4.2/μm^2); filament length, 1 μm; persistence length, 8 μm; time interval, 0.1 s. (B) Direction change of filaments toward the reference axis. The direction was categorized into 8 sub-divisions at intervals of 45° (blue dashed lines). The division of the largest population (orange region) was selected, and the average direction in the selected division was subsequently determined as the reference axis (long red arrow). (C) Change in the moving direction of all actin filaments toward the reference axis (determined by the average direction) according to variation in the packing ratio, P. Bidirectional movement was permitted. (D) Translation of a filament into the nearest filament with a bias distance.

This operation was conducted for all filaments. Finally, the initial constraint was set so that all filaments were initially positioned at random but directed along the *x*-axis with Gaussian distribution (SD ±15° based on the *x*-axis). The right and left directions of filaments were set at the same probability.

2.3 Parameters depending on KCl concentration

The sliding velocity of actin filaments depends on the KCl concentration to achieve control of ionic strength. In addition, the driving force of myosin motors decreases with the increase in KCl concentration. We estimated the driving force in the simulation from experimental data, as depicted in Fig. 4. In a motility assay, the driving force toward the longitudinal direction of filaments was measured to be 4 pN/μm of filament at 25 mM KCl[13]. The maximum tension of muscle fibers showed an almost perfect linear decrease and reduced by half in the range of 25–150 mM KCl[14]. In the presence of dense MC, a packing force is likely to occur among filaments due to a possible excluded volume effect. Here, we supposed the packing force to be 2 pN per filament in line with the experimental results (see Sec. 4.4 for a discussion on the validity of this value). The packing ratio parameter P was calculated by $P = \tan^{-1}$(packing force/driving force)/90°. The values of velocity, driving force, and parameter P as a function of KCl concentration are summarized in Table 1, which were applied to the simulation. The average velocity was obtained from data of the previous study[9] as: average velocity of moving filament × moving ratio.

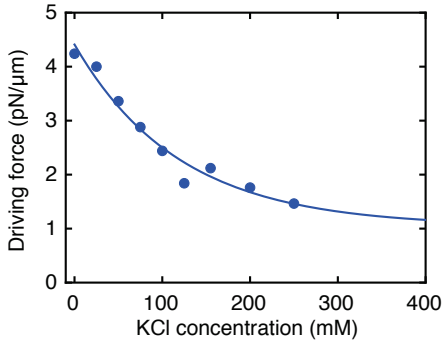

Figure 4: Estimation of the driving force depending on KCl concentration, based on data from in vitro motility and muscle fiber experiments. The driving force of myosin for sliding actin filaments at 25 mM KCl in an in vitro motility system was obtained from reference[13], and the dependence of tension in muscle fibers on KCl concentration is derived from references[11,14].

2.4 Evaluation of pattern formation

To evaluate the collectivity level, a

Table 1: Parameters in response to KCl concentrations.

Parameters	KCl concentration (mM)							
	0	25	50	100	150	200	300	400
Velocity (μm/s)*	4	6	8	6	6	4	2.5	2
Driving force (pN/μm)**	4.2	3.8	3.3	2.5	2	1.7	1.3	1.1
Packing ratio, P	0.28	0.31	0.34	0.43	0.5	0.56	0.63	0.68

*Values were obtained from reference[9].

**Driving forces were obtained from Fig. 4.

condensation index was defined according to Shannon entropy (S) as follows:

$$S = -\frac{1}{N}\sum_{i=1}^{N} \Delta\rho_i \log \Delta\rho_i \,,$$

where N is the total number and $\Delta\rho_i$ is the relative density around the i-th filament compared to the average density.

While filaments assembled into stream bands, they tended to align at regular intervals. The distance between the centers of the bands was measured as the space interval. For each condition, the simulation was independently performed 20 times with different random numbers.

3. Results

3.1 Condensation of moving actin filaments

The target phenomenon being simulated is the alignment patterns of bands composed of myosin-driven actin filaments (Fig. 1). Fundamentally, the simulation required initially setting a directed distribution of filaments (see Sec. 2.2, initial constraint). By applying a random direction as the initial constraint, the system became unstable and all filaments tended to gather into a single large stream.

When parameters E, P, and average velocity (V) were set to 1.4, 0.56, and 4 μm/s, respectively, which were expected from the condition of 200 mM KCl, the filaments

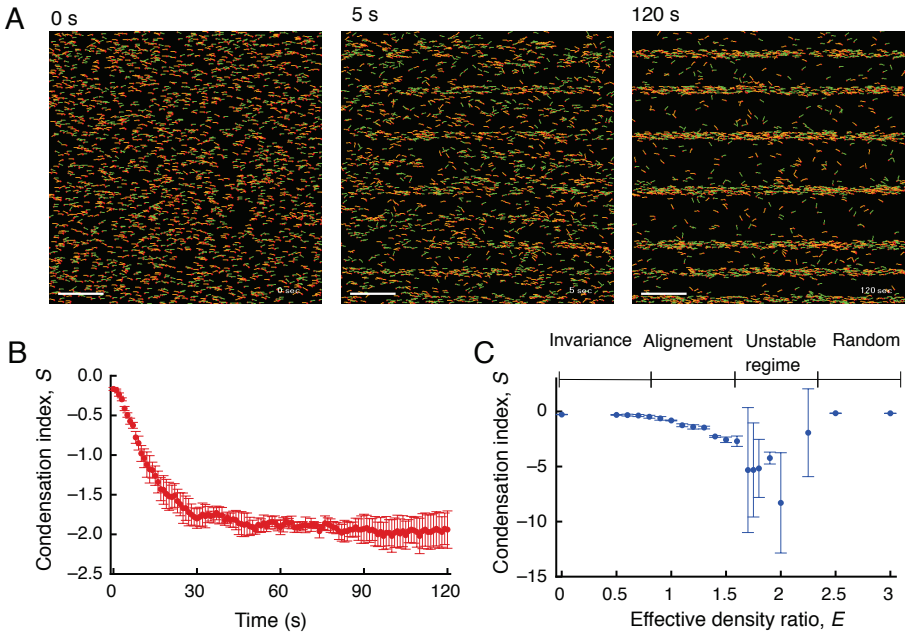

Figure 5: Simulated stream band formations. (A) Time sequential images of pattern formation in the expected conditions of 200 mM KCl. Green and orange represent left-directed and right-directed filaments, respectively. Elapsed time is indicated at the top left of each panel. Scale bar, 10 μm. (B) Time development of the condensation of filaments. Filament number, 15,000; E, 1.4; P, 0.56; V, 4. (C) Dependence of condensation on parameter E. Data were obtained after 120 s. Error bars indicate the standard deviation (n = 20).

gathered into narrow bands and distinct alignment of bands occurred as well as formation of a striped pattern (Fig. 5A). The condensation index *S*, with negative values indicating predominant condensation, decreased as time elapsed (Fig. 5B). Local condensation became apparent for 5 s and the alignment bands reached maturity after 50 s.

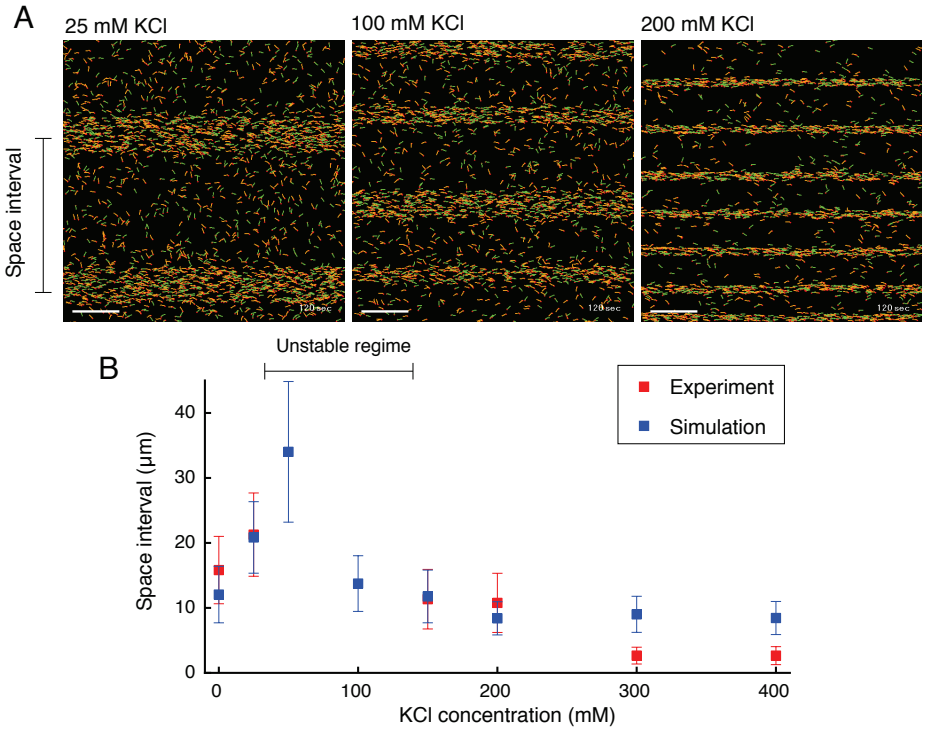

Figure 6: Pattern formations in response to KCl concentrations. (A) Images of patterns formed with KCl concentrations of 25 mM, 100 mM, and 200 mM. Scale bar on the bottom left, 10 μm. (B) Space interval between aligned bands *versus* KCl concentration. Blue and red squares indicate data from the simulation and experiment[9], respectively. Error bars indicate the standard deviations (n = 20). An unstable regime means that the streams meandered without obvious direction or alignment in the experiment.

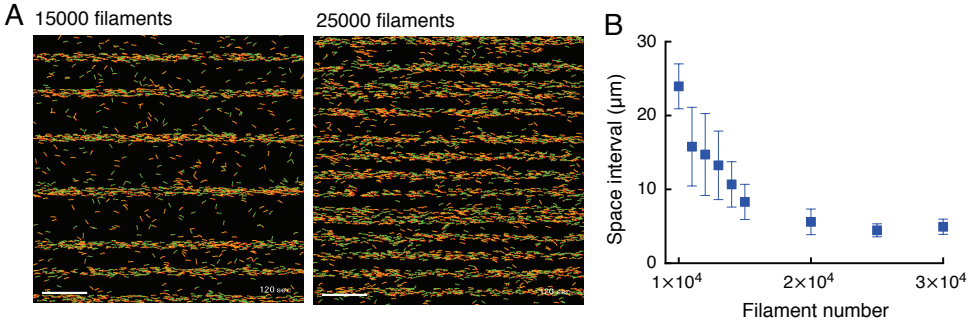

Figure 7: Dependence of space intervals on filament number, *N*. (A) Images of simulated patterns formed with 15,000 (left) and 25,000 (right) filaments under a condition of 200 mM KCl. Parameter *E* was varied in response to *N* (see Sec. 4.2). (B) Space interval *versus* filament number. Error bars indicate standard deviations (n = 20).

The parameter *E*, which represents the threshold value for effective density, was important for the condensation behavior (Fig. 5C). The striped pattern was observed in the *E* range of 0.5–1.6, whereas the setting of 1.7–2.2 often induced formation of a large single tide of actin filaments, which was unstable (i.e., showed different features in repeated tests). With an *E* value above 2.3, each filament non-directionally moved without band formations, whereas at *E* values below 0.5, the filament movement pattern did not deviate from the initial situation.

3.2 Alignment of stream bands of actin filaments

Next, we examined the dependence of alignment on *P* and *V* when *E* was fixed at 1.4, which was found to induce stable alignment in the system. The combinations of *P* and *V* with respect to variation in the KCl concentration are shown in Table 1. Figure 6 demonstrates the simulated dependence of the space intervals of the aligned bands on the putative concentrations of KCl in comparison to experimental data. As the KCl concentration increased from 0 to 50 mM, the magnitude of space intervals increased from 12 to 34 μm, and the band width became more narrow. At a KCl concentration of 75 mM, the intervals reached the maximum level and the formation was unstable (i.e., different features containing large single tides in repeated tests), resulting in large SDs. At even higher KCl concentrations, the interval decreased down to 9 μm and the bands tended to align. When the total filament number was increased and the *E* value decreased, the space interval became shorter (Fig. 7).

3.3 Other aspects of collective movement

The proposed model provides an explanation not only for the alignment of band formations but also for the collective movement observed as a rank reported by other groups[4,5]. This collective movement was simulated when the bidirectional constraint was invalid and the parameters *P*, *E*, and *V* were set to 0.1, 1.4, and 5, respectively (Fig. 8). In this case, a small *P* (< 0.1) was sufficient for formation of a robust collective, which was not largely influenced by variations

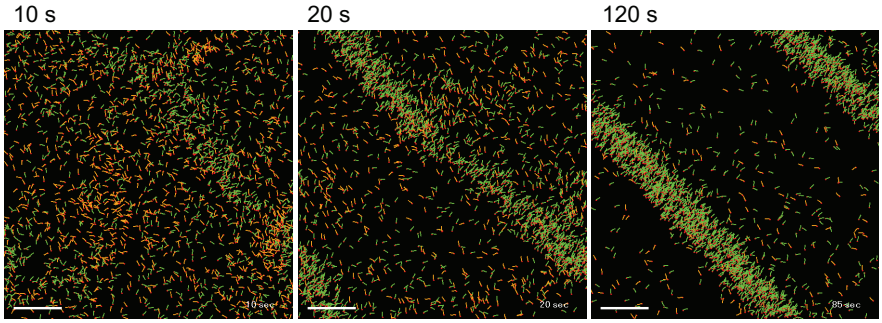

Figure 8: Collective movement of actin filaments in a rank. Conditions: velocity, 5 μm/s; *E*, 1.4; *P*, 0.1. Bidirectional permission was invalidated.

of E and V in contrast to the case of alignment formations.

4. Discussion

4.1 Requirements for a well-reproduced simulation

The present simulation required the following three main assumptions. First, the moving direction of actin filaments was altered by the population of neighboring filaments due to an uncertain mechanism. Each filament was translated to the nearest filament as a function of both P and the angle between filaments, although this was a simplistic assumption without a theoretical basis. The operation led to the formation of narrow bands at high KCl concentrations. Even when the assumption was modified, such as using a reciprocal function of distance, alternation of space intervals between the formed bands was obscure.

Second, assumption of a certain filament density was required for alternation of movement. In this situation, bidirectional constraint was permitted (i.e., the actin filament could turn within ±90° based on a reference axis). In fact, experiments have shown that two anti-parallel actin filaments can move alongside each other without slowing down to form narrow bands of actin filament streams.

Finally, at the initial time, the actin filaments were assumed to be directed toward the x-axis with Gaussian distribution because a setting of complete random direction resulted in large condensation without creation of narrow bands. Experimentally, aligned bands tend to be oriented parallel to the flow direction by a perfusing solution, which supports the initial assignment.

4.2 Implication of filament density for condensation and band formation

In the simulation, we took into consideration the effect of how the packing force is applied on filament movement. Experiments demonstrated that a high density of filaments (~20 filaments/μm^2) is essential for establishing collective movement[4]. At low density, each filament independently migrates, and the individual directions can be slightly affected by those of the opponents, while two moving filaments tend to collide with each other[15]. By contrast, the high density conditions induce ordered pattern formations, in which cooperative phenomena (via an unknown mechanism) resulting from multi-filament collision may be required[16].

In the present simulation study, we set the filament density to 4.2/μm^2 because our previous finding[9] was obtained at a 5-times lower density compared with that used in the above-mentioned study[4]. We then assumed a threshold density for establishing a packing effect among numerous filaments. When the threshold was not applied (E = 0, the packing effect was enabled at all times), the average direction (reference direction) was determined according to the initial distribution due to counteracting effects among many filaments. In this case, no obvious band formation was observed during the 120-s simulation. However, when the threshold density was 0.8–1.5 times the average density, stable band

formation occurred. At a critical point (E = 2.0) before transiting to random movement, the system became unstable and large condensation forms appeared. It is likely that E determined the number of nuclei required for the growth of bands. These results indicate that local density fluctuation is crucial for aligned band formation. We also examined the contribution of the total number (or average density) of filaments to the pattern formations. When E was fixed at a constant value of 1.4, the condensation index and space intervals were almost completely unchanged by variations in the total filament number. If the effective density was assumed to be an absolute value (according to the criterion: density 4.2/μm^2 × (E: 1.4) = 5.8/μm^2), the increase in the total number of filaments (10,000–25,000, i.e., 2.8–7.0/μm^2) would bring about a decrease in the effective density ratio, E (2.1–0.84). In this situation, the increase in total filament number resulted in shorter space intervals between narrow bands, which corresponds to the experimental results[9].

Although the simulation demonstrated that band formations became stable after 50 s, the experiment could not provide data in this time range because the exchange of solutions in a flow cell occurred for 120 s[9]. The experiment showed that bands had already begun to form when the observation was initiated at 120 s. However, after this point, some bands were altered through the collapse or convergence of bands. The time until reaching a steady state might be faster in simulation than in the experiment because the simulation was limited to an area of 60 μm × 60 μm, which is smaller than the actual area (18 mm × 18 mm).

4.3 Space intervals between aligned bands under simulated conditions of KCl concentration

To explain the response to KCl concentrations, parameters were set in terms of variations in KCl concentration, as shown in Table 1. While the filament number and E were constant, the velocity and P were varied. At low KCl concentrations, P was smaller because the driving force tends to be larger under this condition. Some filaments gathered into bands while other filaments moved away from bands, resulting in broad band streams with large space intervals between bands. This result is quite similar to the experimentally observed features. At 50 mM KCl, the stream tended to grow a few large bands by the merging of some bands and space intervals reached their maximum, although these formations frequently became unstable. The experiment also showed that the large bands that formed tended to meander (unstable regime in Fig. 6B). In the range of 100–200 mM, stable band formations occurred and the bands aligned with regular intervals. However, as the KCl concentration increased, the space intervals became shorter, in line with the experimental data. The previous experiment indicated that the space intervals are correlated to the sliding velocity. In the simulation, when the velocity increased during the setting of constant P and E, the space intervals also increased. However, the band formations were unstable and partial

disorder occurred. This result indicates that obvious pattern formation requires not only a change in velocity but also an adequate packing effect. Considerable differences between the experimental and simulation data were found in the condition of a KCl concentration above 200 mM: the intervals in the simulation were unchanged, whereas further shortening of the intervals continued in the experiment. This difference might be caused by the spatial resolution in the simulation. In the simulation, the movement of filaments was evaluated in each search area (2 μm × 2 μm) for applying of the constraint, which is larger than the intervals (1.3 μm) obtained at 300 mM KCl in the experiment. Because the setting of search area influenced the adjustment of other parameters, the optimal spatial and temporal resolutions should be considered further. Overall, our proposed model that the alignment patterns depend on a balance between driving and packing forces could help to considerably explain the experimentally observed phenomena.

4.4 Validity of the estimated packing force

We were confronted with the issue of how to best handle the packing effect in the simulation. One candidate for simulating the packing effect is the depletion force associated with an excluded volume effect. The depletion force as an attraction force was calculated to be roughly 100 pN/μm for two closely packed rigid filaments in corresponding crowded conditions[17]. This value is much higher than the driving force (5 pN/μm). However, at low KCl concentrations, actin bundles assembling in solution can collapse when landing on a myosin-coated surface, suggesting that the packing force is smaller than the driving force in this experimental situation. In addition, with manipulation of single filaments, the depletion force in solution containing a crowder was measured to be within 0.1–3 pN[18]. If separation of two filaments depends on only the motion of the pointed end of a filament, the fracture between filaments is produced by breaking the bonds between monomer units in turn, which is estimated to occur at 2 pN. Thus, we adopted this value for consideration of the competition between the packing force and driving force, which reaches the same level at 150 mM KCl. Although further information is needed to strictly ascertain the packing effect, the value used in the present simulation could well explain the alignment of bands of actin filaments in a motility system under crowded conditions.

4.5 Concluding remarks

We have developed a model for the formation of patterns composed of autonomous actin filaments driven by myosin motors, which are determined by a balance between packing and driving forces as well as velocity. The proposed model is based on certain assumptions without theoretical evidence, and certain limitations remain with respect to the area as well as spatial and temporal resolutions. Nonetheless, the simulation considerably explained the experimental results. Because the simulated

movement of individual filaments was performed on the basis of the movement of actual actin filaments at a time interval of 0.1 s, each parameter might be optimized for the conditions.

Because numerous proteins exist in cells and tissues, it is important to consider the effects of crowded environments when discussing the functions of proteins[19]. In addition, the physiological ionic strength is nearly 200 mM, which has a fair influence on electrostatic interactions between actin and myosin. Such ionic conditions can produce a moderate driving force and maximum velocity of actin filaments, which then suffer from a packing effect due to the presence of crowders. The situation suggests that the formation of aligned actin filaments occurs under a moderate driving force. Other factors such as density fluctuation as well as the balance between different forces might further contribute to the organization of cytoskeletons as observed in cells.

Conflict of interest

The authors declare no conflicts of interest associated with this manuscript.

References

1) A. Mogilner, K. Keren, Curr. Biol. 19, pp. R762–R771 (2009).

2) T.D. Pollard, Curr. Opin. Cell Biol. 22, pp. 50–56 (2010).

3) S.J. Kron, J.A. Spudich, Proc. Natl. Acad. Sci. U. S. A. 83, pp. 6272–6276 (1986).

4) V. Schaller, C. Weber, C. Semmrich, E. Frey, A.R. Bausch, Nature 467, pp. 73–77 (2010).

5) T. Butt, T. Mufti, A. Humayun, P.B. Rosenthal, S. Khan, S. Khan, J.E. Molloy, J. Biol. Chem. 285, pp. 4964–4974 (2010).

6) T. Sanchez, D.T.N. Chen, S.J. DeCamp, M. Heymann, Z. Dogic, Nature 491, pp. 431–434 (2012).

7) A. Saito, T.I. Farhana, A.M.R. Kabir, D. Inoue, A. Konagaya, K. Sada, A. Kakugo, RSC Adv. 7, pp. 13191–13197 (2017).

8) G. Popkin, Nature 529, pp. 16–18 (2016).

9) T. Iwase, Y. Sasaki, K. Hatori, Biochim. Biophys. Acta - Gen. Subj. 1861, pp. 2717–2725 (2017).

10) S. Asakura, F. Oosawa, J. Chem. Phys. 22, pp. 1255–1256 (1954).

11) L. Wang, A. Bahadir, M. Kawai, J. Muscle Res. Cell Motil. 36, pp. 227–241 (2015).

12) R. Shimo, K. Mihashi, Biophys. Chem. 93, pp. 23–35 (2001).

13) M. Kawai, K. Kawaguchi, M. Saito, S. Ishiwata, Biophys. J. 78, pp. 3112–3119 (2000).

14) H. Sugi, T. Abe, T. Kobayashi, S. Chaen, Y. Ohnuki, Y. Saeki, S. Sugiura, PLoS One 8, pp. 1–8 (2013).

15) S. Hussain, J.E. Molloy, S.M. Khan, Biophys. J. 105, pp. 1456–1465 (2013).

16) R. Suzuki, C.A. Weber, E. Frey, A.R. Bausch, Nat. Phys. 11, pp. 1–6 (2015).

17) M. Hosek, J.X. Tang, Phys. Rev. E 69, 51907 (2004).

18) J. Schnauß, T. Golde, C. Schuldt, B.U.S. Schmidt, M. Glaser, D. Strehle, T. Händler, C. Heussinger, J.A. Käs, Phys. Rev. Lett. 116, 108102 (2016).

19) D. Marenduzzo, K. Finan, P.R. Cook, J. Cell Biol. 175, pp. 681–686 (2006).